Supplement for 'An atomtronics transistor for quantum gates'

Miroslav Gajdacz[1,2], Tomáš Opatrný[2], and Kunal K. Das[3]
[1] *Institute for Physics and Astronomy, Aarhus University, Ny Munkegade 120, 8000 Aarhus C, Denmark*
[2] *Optics Department, Faculty of Science, Palacký University, 17. Listopadu 12, 77146 Olomouc, Czech Republic*
[3] *Department of Physical Sciences, Kutztown University of Pennsylvania, Kutztown, Pennsylvania 19530, USA*

In this supplement we provide additional details for this paper. Specifically we illustrate feasibility for our mechanism in two different setups as mentioned in our manuscript: (1) Optical Lattice for single atoms (we present two schemes) (2) Optical dipole traps for aggregates of atoms. We also provide details of our noise analysis.

I. GENERAL CONSIDERATIONS AND ASSUMPTIONS

A. Swappability

A scalable quantum computer requires the operation of swapping two qbits. In our case the two qbits are encoded by two different species. We can ensure swappability of species A and B by sequencing the basic CNOT gate we describe in the paper to create a SWAP gate as follows: SWAP(x, y) =CNOT(x, y)∗CNOT(y, x)∗CNOT(x, y) where CNOT(x,y) transforms $x \to x$ and $y \to x + y$ $(mod 2)$. This requires that we need to be able to *change the role of the two bits*: Each bit must be at least once *controlled* and at least once *controlling*, meaning that the roles of A and B have to be switchable.

We can implement this by using two triple wells that can be switched between two orthogonal 'T-shaped' configuration as shown in Fig. 1 with the dynamics of each species confined to only one direction. The role of the two species can then be switched by simply switching between the two configurations after each cycle. This implicitly requires that *each species is independently trapped by separate species specific potential.* We label the direction of dynamical evolution of the *controlled bit as 'active'* and that of the *controlling bit as 'passive'.*

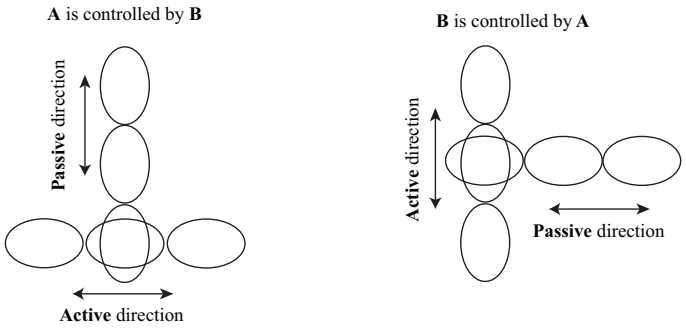

FIG. 1: Scheme for swapping the roles of the two species, with two triple wells, one for each species, in orthogonal T-configuration that can be switched between the two configurations by using different trapping lasers to create the two triple wells.

B. Assumptions

In all that follows, without significant loss of generality we make the following assumptions:

1. We assume the potential transverse to all the triple wells to be sufficiently strong to keep both species 'frozen' in the ground state of their respective transverse potentials.

2. In any given cycle, the depth of the triple-well for the *passive* species can be made sufficiently deep to keep the particle localized in the specific well it happens to be in (one of the two extreme wells, either the one overlapping with the central well of the active direction or the one at the other extreme).

3. Due to the previous two assumptions, *all our simulations will be in effective 1D along the 'active' direction with co-ordinate "z". For simplicity of notation we will refer to the controlled species as A and controlling species as B*

4. We assume the transverse trapping potential to be cylindrically symmetric 2D harmonic trap and denote directions *transverse to the direction of the triple wells* by "$\perp$".

II. OPTICAL LATTICE: SINGLE PARTICLE OF EACH SPECIES

In the case of optical lattices the triple wells are formed by a three harmonic component super-lattice, where the third harmonic is generated by counter-propagating beams with wavelength λ and the first and second harmonics are obtained by using the same light now intersecting at an angle as to increase the spatial periodicity of the interference pattern along the triple-well direction. We assume a *single particle of each species*. Integrating out the transverse wavefunction, we get an effective 1D 2-particle Hamiltonian for hard-core bosons, with 'a' being the inter-species scattering length:

$$\hat{H}_{long} = \frac{-\hbar^2}{2m_A}\frac{\partial^2}{\partial z_A^2} + \frac{-\hbar^2}{2m_B}\frac{\partial^2}{\partial z_B^2} + V(z_A, z_B) + 2a\hbar\omega_\perp\delta(z_1 - z_2) \tag{1}$$

We choose our length unit to be $l = \lambda$ for the active species A and the *energy unit* $\varepsilon = E_R = h^2/(2m_A\lambda^2)$ the corresponding recoil energy and time unit $\tau = \hbar/\varepsilon$ and denote $l_\perp = \sqrt{\hbar/(m_A\omega_\perp)}$ the transverse oscillator length for species A. Using a common transverse trapping frequency $\omega_\perp$ for both species, we reduce it to a dimensionless form:

$$\hat{H}_{long} = \frac{-1}{(2\pi)^2}\frac{\partial^2}{\partial z_A^2} + \frac{-1}{(2\pi)^2}\frac{m_A}{m_B}\frac{\partial^2}{\partial z_B^2} + V(z_A, z_B) + \frac{a}{\pi^2 l_{\perp A}^2}\delta(z_1 - z_2). \tag{2}$$

Note: We present two lattice designs which differ only in the potential experienced by species B. So the **evolution of species A is the same for both**. Only the evolution of species B is a bit different with little effect on species A.

A. Lattice design 1: Swappable

This design is suitable for direct implementation of the swappable configuration shown in Fig. 1 assuming two distinct species ^{87}Rb and ^{23}Na with respective trapping wavelength $\lambda_{Na} = 600$ nm and $\lambda_{Rb} = 800$ nm along the active directions for each. With ^{23}Na, $D1, D2 \simeq 589$ nm lines and ^{87}Rb $D1 = 795$nm, $D2 = 780$nm so this ensures each species is red-detuned by about 10 nm from its trapping frequency, but far off-resonant from that of the other.

Parameters: We present the relevant parameters in Tables I and II for ^{87}Rb and ^{23}Na as the active species respectively (the units ε and l are therefore different). We consider two different transverse lattice depths of $V_\perp = 60\varepsilon$ and $V_\perp = 80\varepsilon$ accessible in current experiments. The interspecies scattering length of ^{23}Na and ^{87}Rb is 103 a_B [1]. Along the direction of the triple-wells, the well depths never exceed $V_z = 20\varepsilon$.

We use $\omega_\perp = (2\pi/\lambda)\sqrt{2V_\perp/m_A}$ for the effective harmonic oscillator angular frequency of the transverse potential, and note that in our units $l_\perp$ and the transverse confinement energy $2\hbar\omega_\perp$ depend only the depth of the potential.

TABLE I: ^{87}Rb as active species $l = \lambda = 800$nm

parameter	$V = 80\varepsilon$	$V = 60\varepsilon$
Energy unit $\varepsilon = E_R$	2.36×10^{-30} J	
Time unit $\tau = \hbar/\varepsilon$	4.47×10^{-5} s	
Transverse trap freq. $\omega_\perp$	4.0×10^5 Hz	3.5×10^5 Hz
Int. strength g_{1D}	$0.244\ \varepsilon \cdot l$	$0.211\ \varepsilon \cdot l$
Transverse Osc. Length $l_\perp$	$0.053\ l$	$0.057\ l$
Transverse energy $2\hbar\omega_\perp$	$36\ \varepsilon$	$31\ \varepsilon$
Int. energy g_{1D}/l_z	$3.24\ \varepsilon$	$2.8\ \varepsilon$

TABLE II: ^{23}Na as active species $l = \lambda = 600$nm

parameter	$V = 80\varepsilon$	$V = 60\varepsilon$
$\varepsilon = E_R$	1.6×10^{-30} J	
$\tau = \hbar/\varepsilon$	6.7×10^{-6} s	
$\omega_\perp$	2.7×10^6 Hz	2.33×10^6 Hz
g_{1D}	$0.325\ \varepsilon \cdot l$	$0.281\ \varepsilon \cdot l$
$l_\perp$	$0.053l$	$0.057l$
$2\hbar\omega_\perp$	$36\ \varepsilon$	$31\ \varepsilon$
g_{1D}/l_z	$4.3\ \varepsilon$	$3.74\ \varepsilon$

Salient Points: We summarize the primary implications of these estimates:

1. Our use of $g_{1D} = 0.26\ \varepsilon \cdot l$ in the paper is justified by realistic parameters.

2. Time scale for operation is about 11.86 τ which translates to 0.53×10^{-3}s for active ^{23}Rb and 0.079×10^{-3}s for active ^{23}Na, implying sub-millisecond operation time scales, comparable to or better than most proposed schemes for quantum gate.

3. Effective 1D dynamics or species A is justified: The transverse energy $\sim 30\varepsilon$ is much higher than the sum of the longitudinal kinetic energy $\sim \varepsilon$ and interaction energy $g_{1D}/l_z \simeq 4\varepsilon$. The latter is estimated by the product of the interaction strength and 1D particle density $\sim N/L \simeq 1/l_z$ with $N \sim 1$ since we consider single particle of each species; the extent of the density overlap of the particles during evolution is estimated by the effective *longitudinal* oscillator length $l_z = \sqrt{\hbar/(m_A\omega_z)}$ where $\omega_z = (2\pi/\lambda)\sqrt{2V_z/m_A}$ we take $V_z = 20\varepsilon$ as the upper limit of the longitudinal depth of the wells as seen in Fig. 4.

B. Lattice design 2: Not Swappable

We also present an alternate design which will not allow swapping but can be easier to implement in an experiment since it requires fewer trapping beams and can be implemented with a single atomic species. We take two spin states of ^{87}Rb $|F = 1, m_F = 1\rangle$ state for species A and $|F = 2, m_F = 2\rangle$ state for species B. We will choose the second harmonic to be the $\sigma^{(-)}$ polarized light at the 'magic' wavelength 785 nm [2], at which it is *invisible* to species B in state $|F = 2, m_F = 2\rangle$ due to the cancelation of the D1 and D2 line polarizabilities which have equal strength but opposite signs. On the other hand, 785 nm is red-detuned for species A $|F = 1, m_F = 1\rangle$ which therefore sees an attractive potential.

Then we take the first and the third harmonics to be far detuned from both species such that they have the same strength for both. As shown in Fig. 2 the absence of the second harmonics results in a much deeper central well for species B. Even when the lattice depth is varied as part of our dynamic mechanism, species B remains well-localized in the center, provided it was prepared in a local ground state of that well. We find in our simulations (shown in Figs. 3 and 4) that the dynamics can be made almost the same as in the model presented in the paper.

Parameters: The scaled Hamiltonian is given by Eq. (2) with $m_A = m_B$. Taking the transverse lattice depths of $80E_R$ and using the triplet scattering length of ^{87}Rb, $a = 99a_B$, we get values for the parameters $\omega_\perp = 9.4 \times 10^5$Hz, $l_\perp = 5.3\lambda$ and $g_{1D} = 0.36E_R \cdot \lambda$ which are similar to those for the *lattice design 1*.

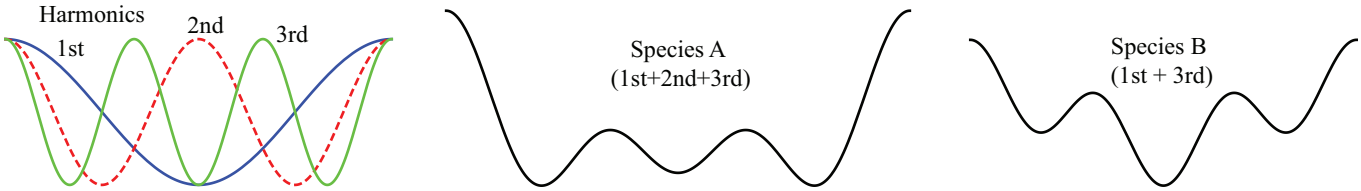

FIG. 2: **Species Selective Potentials for Lattice Design 2:** Schematic is shown for (a) Three harmonics, corresponding to lattice periodicities $3\lambda/2, 3\lambda/4, \lambda/2$, the 1st, 2nd and 3rd harmonics respectively; (b) Potential seen by species A with all three contributing, (c) potential seen by species B, with only 1st and 3rd harmonic contributing. [Here equal amplitudes are assumed for all harmonics to illustrate the scheme, but in practice the amplitudes will vary].

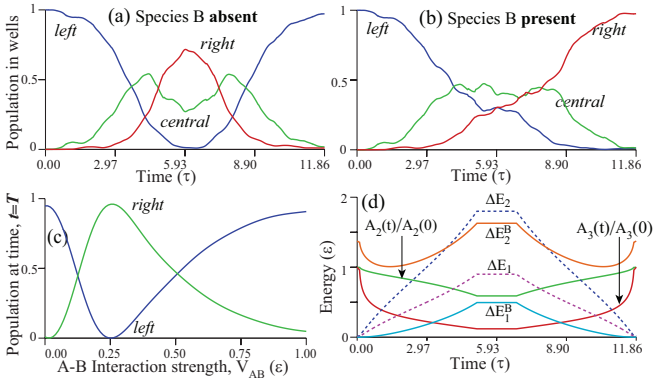

FIG. 3: **Equivalent of Fig. 3 in the resubmitted manuscript (Fig. 4 in the first submitted version) but here it is for a lattice potential**. Comparison confirms the behavior is essentially the same. The primary difference is that in plot (d) here we plot the **amplitudes** $A_2(t), A_3(t)$ of the time variations of the second and the third harmonics instead of the barrier heights and separation for the triple-well presented in the paper. Also the units are different.

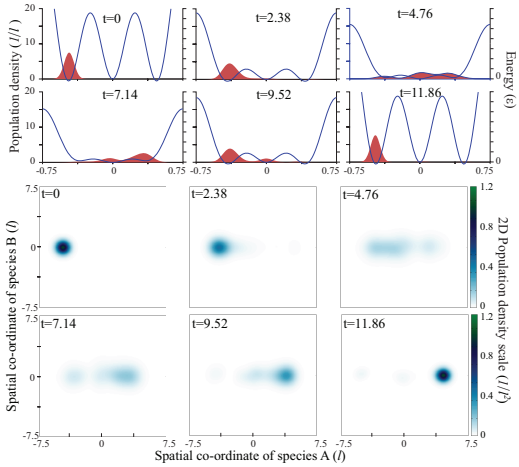

FIG. 4: **Equivalent of Fig. 4 in the resubmitted manuscript (Fig. 5 in the first submitted version), but here it is for a lattice potential**. Comparison confirms that the behavior is essentially the same. The primary difference is that due to our assumption of lattice design 2, the species B has a somewhat broader density distribution, but remains well localized as we require.

III. TRIPLE WELL: USING BEC OF EACH SPECIES

Main Design goals: Our design incorporates the following essential features:

(i) Species A has none or negligible self-interaction so that its eigenstates can be defined by the linear Schrödinger equation.

(ii) Interspecies interaction between species A and B is in the range necessary for our mechanism, not too strong and not too weak.

(iii) The confining potential is species selective.

(iv) Both species have sufficient number of atoms (≥ 1000) to allow use of mean field theory (this is not essential, but mainly assumed to conduct our numerical estimates here).

(v) Both species are trapped in such a way that the dynamics is effectively one-dimensional.

(vi) Spatial extent of species B along the direction of transport remains well localized within acceptable limits as defined in our mechanism.

Swappability: In order to implement swappability as described earlier, we need to take into account that the active species has to be non-interacting, which can be done with Feshbach resonance. Since the magnetic field can be tuned to make only one species non-interacting (baring some extraordinary coincidence), the magnetic field will have to be tuned to the Feshbach resonances for whichever species is active, when the roles of the species are switched. When one wishes to cancel the self interaction of a species with narrow Feshbach resonances such as Rb, this becomes an experimentally non-trivial requirement, however in principle it can be done, particularly considering the variety for species-pairs that are being currently trapped. In what follows we will fix one species as active and the other as passive to demonstrate feasibility.

Design: For species A we pick ^{7}Li and species B to be ^{87}Rb, both bosonic and assumed to be in degeneracy. To allow magnetic tuning to Feshbach resonance, we assume an optical dipole trap. Experiments [3] have shown that ^{7}Li in $|F = 1, m_F = 1\rangle$ state has a very weak scattering length $a = -1 * a_B$ at 560G and changes sign and goes up to $a = 10a_B$ at 630G. This implies that it has zero scattering length at about 566G (by linear interpolation). On the other hand the theoretical studies have computed inter-species s-wave scattering length [4] between ^{7}Li in $|F = 1, m_F = 1\rangle$ and ^{87}Rb in $|F = 1, m_F = 1\rangle$ is zero at 438G and positive above that until it hits resonance at 566 G (coincidentally!). That coincidence in field strength means that we cannot be exactly at 566 G necessary for $a = 0$ for Lithium, but we find that we can tune the interspecies scattering to around $a = +100\ a_B$ at 560 G by being close but not quite at the resonance while having the species A scattering length of the order of $a = -1\ a_B$, which is low enough that it has negligible effect on the dynamics or eigenstates of species A. Notably, the magnitude of the interaction can be further decreased but at the cost of increasing the interspecies interaction. We introduce two novel design features:

1. Both species are confined by the same optical dipole trap in longitudinal direction (direction of dynamics). However, the two Gaussian barriers that create the triple well structure are only felt by species A, which can be achieved by keeping the frequencies of the lasers that create them far off-resonant with respect to the species B, ^{87}Rb. As we will show, species B is sufficiently well localized even without the two barriers and there is the advantage that variation of the barriers do not affect species B at all.

2. We allow for a small relative transverse offset of the longitudinal axes of the two species, which allows adjusting the degree of overlap of the two species, providing an additional parameter to control the inter-species interaction.

Parameters: We consider a geometry in which the Rb and Li are confined in a cigar-shaped optical dipole trap by the *same* longitudinal laser that we choose to be of 1064 nm wavelength. The two species will still experience different axial trap frequencies due to different detuning and masses. The tight transverse confinement implies a Gaussian shape transverse profile for both species (i =A,B labels the species): $\Phi_i(r_i, z_i) = \sqrt{2\beta_i} e^{-\beta_i r^2/2}\psi_i(z_i)$. Integrating out the transverse direction we get the dimensionless coupled effective 1D Gross-Pitaevskii equations:

$$\begin{aligned} \frac{1}{2}\left[-\frac{\partial^2}{\partial z_A^2} + z_A^2\right]\psi_A + \frac{a_{AB}N_B\beta_B}{\mu_{AB}}|\psi_B|^2\psi_A &= i\partial_t\psi_A \\ \frac{1}{2\mu_B}\left[-\frac{\partial^2}{\partial z_B^2} + \mu_B^2\eta_z^2 z_B^2\right]\psi_B + \frac{a_{AB}\beta_A N_A}{\mu_{AB}}|\psi_A|^2\psi_B + \frac{2a_{BB}N_B\beta_B}{\mu_B}|\psi_B|^2\psi_B &= i\partial_t\psi_B \end{aligned} \tag{3}$$

As described above, the self-interaction of species A is set to be zero. Here we have taken the axial frequency ω_z^A of

species A to define our units: $energy \rightarrow \varepsilon = \hbar\omega_z^A; length \rightarrow l = \sqrt{\frac{\hbar}{m_A\omega_z^A}}; time \rightarrow \tau = (\omega_z^A)^{-1}$, and have defined:

$$\frac{\omega_\perp^B}{\omega_\perp^A} = \eta_\perp; \qquad \frac{\omega_z^B}{\omega_z^A} = \eta_z; \qquad \frac{m_{AB}}{m_A} = \mu_{AB}; \qquad \frac{m_B}{m_A} = \mu_B; \qquad l_\perp^B = \frac{1}{\sqrt{\mu_B\eta_\perp}} l_\perp^A, \tag{4}$$

where m_{AB} is the reduced mass of species A and B, and $l_{\perp(z)}^{A(B)}$ are the respective harmonic oscillator lengths, a_{ij} the s-wave scattering lengths, N_i the number of atoms.

We take the trap frequencies for Rb to be $\omega_z^B = 2\pi \times 10$ Hz and $\omega_\perp^B = 2\pi \times 100$ Hz and take the Li transverse trap frequency to be $\omega_\perp^A = 2\pi \times 1000$ Hz, while its longitudinal frequency is fixed by ω_z^B since the same laser wavelength is used. We take the number of atoms for both species to be $N_A = N_B = 1000$, large enough to justify the mean field theory used here [5], but not so large as to create phase fragmentation in elongated traps. Then using the ratio of detuning for the two species $\frac{\delta^A}{\delta^B} = 1.6$ in the longitudinal optical trapping field, we have:

$$\eta_\perp = \frac{\omega_\perp^B}{\omega_\perp^A} = \frac{1}{10} \qquad \eta_z = \frac{\omega_z^B}{\omega_z^A} = \sqrt{\frac{\delta_z^A}{\delta_z^B}\frac{m_z^A}{m_z^B}} = \frac{1}{2.78} \qquad \frac{l_z^B}{l_z^A} = \sqrt{\frac{m_z^A\omega_z^A}{m_z^B\omega_z^B}} = \frac{1}{2.11} \qquad \frac{l_\perp^B}{l_\perp^A} = \sqrt{\frac{m_\perp^A\omega_\perp^A}{m_\perp^B\omega_\perp^B}} = \frac{1}{1.12}. \tag{5}$$

As will be justified shortly, the interspecies coupling term in the species B equation is small relative to its self-interaction, so it does not have any significant influence in determining the properties of species B. By neglecting it we have a simple GP equation for Rb. Following Ref. [5], we assume a Thomas-Fermi profile in the z-direction, justified because of weak trapping along it: $\psi(z_B) = \sqrt{3/(4d_B^3)}\sqrt{d_B^2 - z_B^2}$, where $z_B \in [-d_B, d_B]$. We determine the values of the relevant parameters by minimizing with respect to parameters β_B and d_B the resulting Gross-Pitaevskii energy functional corresponding to the Rb equation above *without the cross-interaction term*

$$\frac{E[\Phi_B]}{N} = \eta_z \left[\frac{1}{2\mu_B\eta_z} \left(\beta_B + \frac{(\mu_B\eta_z\gamma_B)^2}{\beta_B} \right) + \mu_B\eta_z \frac{d_B^2}{10} + \frac{1}{\mu_B\eta_z} \frac{3N_B a_{BB}\beta_B}{5d_B} \right]. \tag{6}$$

TABLE III: Units

Physical unit	**value**
Energy unit $\varepsilon = \hbar\omega_z^A$	1.8×10^{-32} J
Length unit $\sqrt{\frac{\hbar}{m_A\omega_z^A}}$	7.2×10^{-6} m
Time unit $(\omega_z^A)^{-1}$	5.7×10^{-3}s

TABLE IV: Summary of parameter for two-species BEC in triple-well

parameter	**dimensionless value**
Transverse size of B is $l_\perp^B = \sqrt{1/\beta_B}$	$\beta_B = 35.85 \simeq 36 \quad \Rightarrow l_\perp^B = 0.17\ l$
Transverse size of A is $l_\perp^A = \sqrt{1/\beta_A}$	$\beta_A = 35.97 \simeq 36 \quad \Rightarrow l_\perp^A = 0.17\ l$
Longitudinal size of B is	$d_B = 1.58\ l$
Longitudinal size of A is	$l_z^A = 1\ l$ (by choice of units)
chemical-potential of B	5.7 ε less than $2\hbar\omega_\perp^B = 7.2\ \varepsilon$)
Self-interaction strength of B	$\frac{2a_{BB}N_B\beta_B}{\mu_B} = 4.2\ \varepsilon \cdot l$
Cross-interaction strength for A	$\frac{a_{AB}N_B\beta_B}{\mu_{AB}} = 28.6 \simeq 29\varepsilon \cdot l$
Cross-interaction strength for B	$\frac{a_{AB}N_A\beta_A}{\mu_{AB}} = 28.7 \simeq 29\varepsilon \cdot l$

We summarize the results in Table IV. The cross-interaction turns out to be much higher than the self-interaction for species B, contrary to our assumption. Likewise the cross-interaction for species A is two orders of magnitude higher than is assumed in our simulations. We rectify this by creating a slight transverse offset of the longitudinal axes to reduce the overlap of the two species. Since the radial profiles are identical for the two, we can get the geometric factor by integrating:

$$\int_{-\infty}^{\infty} dy e^{-\beta y^2} \times \left[\int_{-\infty}^{d/2} dx e^{-\beta(x-d)^2} + \int_{d/2}^{\infty} dx e^{-\beta x^2} \right] = \frac{\pi}{\beta} Erfc[d\sqrt{\beta}/2] \tag{7}$$

which is an Error-Function and where we find the line of intersection of the surfaces by setting $x^2 = (x-d)^2 \Rightarrow 2x = d$ for positive offset d. So we numerically solve (for $\beta = 36$):

$$29 \times \frac{\pi}{\beta} Erfc[d\sqrt{\beta}/2] = 0.5 \qquad\qquad d = 0.304l \tag{8}$$

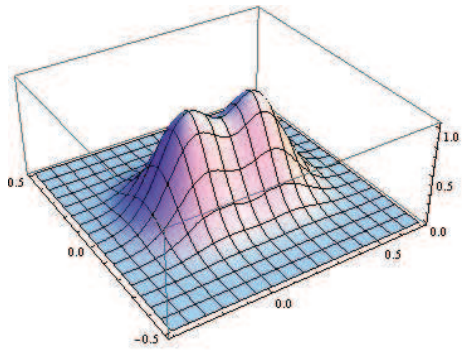

FIG. 5: Plot of the two offset Gaussian for the parameters $d = 0.304, \beta = 36$

The radial densities are shown in Fig. 5 and as can be seen even a small offset leads to a significant reduction of the interspecies interaction.

Salient points: We summarize the primary implications of these estimates:

1. Our use of $g_{1D} = 0.5\ \varepsilon \cdot l$ assumed in the paper can be realized with BEC's by offsetting their axes.

2. The spatial extent of species B is $2d_B \simeq 3l$ which is more localized than the size we assume for the central well in the paper, $2d \simeq 4l$, measured as the separation between the peaks of the barriers.

3. The dynamics along the active direction is effectively 1D since the chemical potential of even species B (which has interaction) is 5.69ε which is less than the energy required for exciting the 1st transverse excited state 7.2ε.

IV. ESTIMATE OF GATE ROBUSTNESS

We describe the roubustness of our proposal in the context of the quantum gate operation since that is less tolerant than the transistor. We consider the two primary sources of fluctuations and errors in the outcome: (i) Coupling to states outside the three-state manifold assumed (ii) fluctuations of the physical parameters.

Coupling to Higher energy states: In our simulations we have found 98% fidelity for the triple well case and *lattice design 1*, and 96% fidelity with the lattice design 2 described earlier, in both the dynamic and the static case. The infidelity is primarily due the effects of the higher lying states. In the static case the fidelity would have been 100%, if we had chosen the initial state be a strict superposition of the lowest three eigenstates since the Hamiltonian does not evolve. But we used a Gaussian initial state to show that a well-localized state can be projected almost entirely onto the lowest three states.

The primary advantage of the dynamic case is that it allows us isolating the initial and final state for initiation and readout. The trade-off is the coupling to higher lying states introduced by the time-dependent potential. But the energy difference between the highest of the three state manifold with the next higher state is about 10 times the energy separations within the manifold. This allows the evolution to be non-adiabatic with respect to the manifold energies, while maintaining adiabacity with respect to the coupling to higher lying states. This allowed us to match the fidelity of the static case, and by a choice of just 20% stronger interaction obtain a time scale identical to that resulting from the natural phase evolution of the eigenstates in the static potential.

Fluctuations of the physical parameters: In optical traps, such as we consider, there can be (i) high frequency noise (>kHz) related to the lasing system and controlling electronics, and (ii) low frequency noise ≤ 100 Hz due to vibration of optical elements or static errors due to imprecise calibration of laser powers. The high frequency noise typically leads to heating. In the case of the lattice implementation, the operation times are $0.1 - 0.5$ ms, and single atoms can be trapped in lattices ~ 10 s [6]. Therefore the loss of fidelity due to such noise $\sim 10^{-4}$. For implementation with BEC, for our choice of parameters the operation times are $44\tau = 0.25$ s, which is slow compared to the lattice, and heating effects can be significant. But BEC of various species have been created with lifetimes [7, 8] ranging $10 - 100$ s, and moreover our operation can speeded up by using tighter traps, whereby such effects could be reduced to $< 1\%$. Since BEC of 10^6 atoms [9] has been shown in experiments to have a lifetime 18 s, therefore with much lesser atoms 10^3 as we assume, the lifetimes can be much longer and therefore loss due to heating proportionately smaller. For gate operation, the lattice implementation is still clearly the preferred choice as regards operation speed.

In a lattice, due to short operation time scales low frequency noise can be treated as static deviations in the parameters from the optimal values. Effect of such noise can be best understood if we view the gate operation as an interference effect of the dynamical phase of the three states. At time T, at the end of each cycle, the states 1 and 3 are in phase, so they act like one 'arm' of a Mach-Zehnder interferometer and the state 2, the other 'arm'. The relative phase between the two $\Delta\theta = (\Delta E_2 - \Delta E_1)T/\hbar$ determines the amplitude of the 'outcome' state corresponding to our qubit definition. Therefore the probability and hence the *in*fidelity depends $\bar{f} \propto \sin^2(\Delta\theta)$, and for small deviations, the consequent infidelity is $\bar{f} \propto (\Delta\theta)^2$. The quadratic dependence makes our scheme robust against small amplitude low frequency noises.

We model the effects of the low frequency noise by (i) multiplying specific parameters by $(1 \pm \epsilon)$, with ϵ a small deviation (ii) numerically evolving the cycles with resulting altered amplitudes (iii) compute the second derivative of fidelity by finite-difference. The increase in infidelity is then given by (with i labeling different physical parameters):

$$\Delta\bar{f} = \frac{1}{2}\sum_{i=1}\left|\frac{\partial^2\bar{f}}{\partial\epsilon_i^2}\right|\epsilon_i^2 \tag{9}$$

In typical experiments involving optical traps, it is well known that the phase of the lasers can be made quite stable, so the defining sources of noise are the fluctuations of *amplitude* of the lasers used. We evaluate *six* second derivatives, for each of the three harmonics we need to monitor 2 fidelities: one with and one without species B, they are shown in the table below, provided the amplitudes can be stabilized to $\epsilon_i \sim 0.001$, the absolute increase of infidelity according

derivative	Species B absent	Species B present
$\frac{\partial^2 \bar{f}}{\partial \epsilon_1^2}$	181	126
$\frac{\partial^2 \bar{f}}{\partial \epsilon_2^2}$	272	211
$\frac{\partial^2 \bar{f}}{\partial \epsilon_3^2}$	42	27

to equation (9) is about 2.5×10^{-4}, which is of the same order 10^{-4} as the heating induced infidelity, mentioned above.

The dynamical phases that define our scheme also depend on the cycle time T and the interaction strength V_{AB}. The infidelity dependence is likewise quadratic with respect to the variations in both, given approximately by:

$$\Delta \bar{f} \simeq \left(\frac{\pi}{2T}\right)^2 (\delta T)^2 \qquad\qquad \Delta \bar{f} \simeq \pi^2 (\delta V_{AB})^2. \tag{10}$$

In the case of the interaction, we used the approximately sinusoidal shape of the Fig. 3(a) in the revised manuscript. Even deviations as high as 5% in the time period T leads to only 0.6% deviation in the fidelity, indicating the robustness of the scheme with respect to such fluctuations. The fluctuations in the interaction can be due to that of (i) transverse confining field, which being optical, can contribute similar amplitude noise as above, but with a smaller coefficient, and therefore less than 10^{-4}, and (ii) influenced by magnetic field used for tuning the Feshbach resonances, since the fields can be stable $< 10^{-3}$ [4]this leads to comparable or smaller effects as the other sources of noise.

[1] M. Bhattacharya *et al.*, Eur. Phys. J. D **31**, 301 (2004).
[2] O. Mandel *et al.*, Phys. Rev. Lett. **91**, 010407 (2003).
[3] K. E. Strecker *et al.*, Nature **417**, 150 (2002).
[4] C. Marzok *et al.*, Phys. Rev. A **79**, 012717 (2009).
[5] Kunal K. Das, Phys. Rev. A **73**, 053612 (2002).
[6] M. J. Gibbons *et al.*, Phys. Rev. A **78**, 043418 (2008).
[7] H. Imai *et al.*, Phys. Rev. A **85**, 013633 (2012).
[8] H.-J. Miesner *et al.*, Phys. Rev. Lett. **82**, 2228 (1999).
[9] A. P. Chikkatur *et al.*, Science **296**, 2193 (2002).